

110463

LA-UR-10-05397

Approved for public release;
distribution is unlimited.



Title: Transport by Oscillatory Flow in Soils with Kinetic Mass Transfer, Part I. Theory

Author(s): Donald A. Neeper
Philip H. Stauffer

Intended for: J. of Contaminant Hydrology



Los Alamos National Laboratory, an affirmative action/equal opportunity employer, is operated by the Los Alamos National Security, LLC for the National Nuclear Security Administration of the U.S. Department of Energy under contract DE-AC52-06NA25396. By acceptance of this article, the publisher recognizes that the U.S. Government retains a nonexclusive, royalty-free license to publish or reproduce the published form of this contribution, or to allow others to do so, for U.S. Government purposes. Los Alamos National Laboratory requests that the publisher identify this article as work performed under the auspices of the U.S. Department of Energy. Los Alamos National Laboratory strongly supports academic freedom and a researcher's right to publish; as an institution, however, the Laboratory does not endorse the viewpoint of a publication or guarantee its technical correctness.



**Transport by oscillatory flow
in soils with kinetic mass transfer
I. Theory**

Donald A. Neeper¹ and Philip H. Stauffer²
Earth and Environmental Sciences Division
Los Alamos National Laboratory
Los Alamos, NM 87545, USA

Abstract

The objective of this paper is to provide a design tool for estimating the effectiveness of passive soil vapor extraction, which is the removal of volatile contaminants by barometric pressure variations. This work is applicable to other cases of oscillatory flow in porous media, including tidal aquifers and water or gas flow due to earth tides. Oscillatory flow of a fluid in a porous medium can generate a one-way transport of heat or chemical if there is a gradient of temperature or chemical concentration in an immobile phase. An immobile phase might be provided by soil heat capacity, by stagnant fluid, by sorption, or by dissolution in pore water of soil. The rate of transport is proportional to the square of the amplitude of periodic fluid displacement. Averaged over time, the transport is proportional to the gradient, and is thereby similar to diffusion. As a function of oscillation frequency, the transport rate has a broad peak near the value $\omega\tau_c=1$, in which ω is the angular frequency of oscillation and τ_c is the characteristic equilibration time of the mobile phase with the immobile phase. The analytic theory is presented, along with finite element numerical simulations using actual barometric pressure histories that illustrate application to passive soil vapor extraction.

Keywords: Soil vapor extraction; Transport; Diffusion; Oscillatory flow; Remediation

1. Introduction

This paper explores isothermal axial transport due to oscillatory flow of gas or liquid in a porous medium, with application to the ventilation of soils by barometric pressure variations. Oscillatory flow can increase the transport of heat, dissolved chemicals, or vapor species in the moving fluid, in effect increasing the diffusivity along the axis of flow. This

¹ Guest Scientist and corresponding author. Tel. +1 505 662 4592 *E-mail address:* dneeper@earthlink.net

² Tel: +1 505 665 4638. Fax: +1 505 665 8737. *E-mail address:* stauffer@lanl.gov

transport occurs whenever a mobile phase of a substance (such as a chemical dissolved in water) equilibrates over time with an immobile phase (such as chemical sorbed on the soil matrix), while the mobile phase undergoes oscillatory motion. Although the theory is quite general, we specifically apply it to passive soil vapor extraction (PSVE), in which offending vapors are removed from the vadose zone by barometric pumping of air at an open borehole.

1.1 Review of passive soil vapor extraction

Ellerd, et al. (1999) review PSVE. Jennings and Patil (2002) note that application of PSVE has been hindered by the absence of procedures for estimating its effectiveness. This paper offers such a procedure, expressing the transport as a diffusivity that depends on the period of motion and the rate of exchange between the mobile and immobile phases of the transported substance. We call this the "exchange diffusivity."

1.2 Review of oscillatory flow and transport

Choi and Smith (2005) simulated oscillatory gas advection in soils, finding that ordinary chemical diffusion was greater than effects due to advection. However, they assumed instantaneous equilibration between mobile and immobile phases, thereby neglecting the process that we investigate here. Schonewill (2008) offered an extensive review of the chemical engineering literature related to oscillatory flow. However, his own work examined the dispersion transverse to the flow direction, while the focus of this paper is on transport along the axis of flow. Kay (1977) considered the dispersion of a point source of contaminant during combined tidal and steady estuarine flows. Kurzweg, et al. (1984) analyzed flow in tubes, where the viscous boundary layer of the fluid provides an immobile phase. Nilson et al. (1991) considered barometric air flow in fractured rock, in which the gas-filled porosity between the fractures provides an immobile phase. The analyses of Kurzweg and Nilson depend on the detailed mechanism of the rate-limited exchange between the mobile and immobile phases. In contrast, this paper offers a simplified analysis, in which the exchange between the mobile and stagnant phases is represented by a first-order rate constant, regardless of its physical mechanism. Jaeger and Kurzweg (2003) report removal of vapors from a packed bed by pressure oscillations imposed from one end. They regard the compressible gas oscillations in a packed bed as complicated and "not readily amenable to analytic or numerical calculations." Although analysis of flow in porous media on the

scale of particle size would indeed be complicated, our simplified analytic method uses lumped parameters such as porosity, permeability, and rate constants, representing the situation as a special case of retarded advective transport.

Nonequilibrium transport in soils is often represented as a combination of mobile and immobile phases of the transported substance, as when flow occurs in preferential channels adjacent to stagnant porosity (see, for example, Brusseau, 1994; Wilson, et al., 1995), or when a mobile fluid transports a substance that is sorbed on the immobile soil matrix (Ma and Selim, 1998). Lal and Shukla (2004) and Jury and Horton (2004) discuss rate-limited ("kinetic") sorption. Among others, Armstrong, et al. (1994) and Switzer and Kosson (2007) review rate-limited mass transfer as a cause of the so-called "rebound" of vapor concentration observed during cessation of active soil vapor extraction (SVE). Most previous modeling of SVE has considered rate-limited mass transfer only when coupled to steady, rather than oscillating, flow. Cirpka (2005) considered kinetic sorption during sinusoidal flow, but the results were not applied to practical problems. Although applicable to oscillatory transport in a variety of circumstances, this paper will focus on practical application to soil vapor extraction.

1.3 Outline of this paper

In a previous theory of oscillatory transport (Neeper 2001), the immobile phase had unlimited capacity. Section 2 of this paper expands that theory, allowing finite capacity in the immobile phase. This analysis does not depend on the mechanism of partitioning between the mobile and immobile phases; therefore, it is applicable to almost any physical situation that can be represented by a mobile-immobile nonequilibrium model with oscillatory flow.

In Section 2 we discuss why barometric pumping at a borehole is much more significant than at the plane surface of the ground. For practical design of PSVE systems, we show that the quasi-cyclic advection in a mobile-immobile system can be represented as a location-dependent diffusivity. This enables assessment of the long-term effectiveness PSVE, without requiring simulation of the time-dependent barometric flow and kinetic mass transfer.

Section 3 compares the results of the analytic theory with finite element simulations of flow and transport. Section 3.1 presents a numerical simulation of a soil column for which the results agree with the analytic theory. Section 3.2 presents a simulation in cylindrical geometry, with flow driven by an

actual barometric pressure history. The cylindrical results predict that the barometric frequency spectrum is adequate to enhance the passive extraction of soil vapor in a realistic situation.

Section 4 discusses practical application of the theory.

Section 5 summarizes the conclusions of this paper.

Finally, in a second paper of this sequence (Neeper and Stauffer, this issue) we present analysis of a field experiment for which a mobile-immobile model agrees in detail with time-dependent data.

2. Theory of oscillatory transport in porous media

2.1 The idealized configuration

The oscillatory transport mechanism requires only that mobile and immobile phases of the transported substance both exist, and that they equilibrate at a finite rate. Fig. 1 illustrates idealized one-dimensional mobile-immobile transport systems. Fluid moves with sinusoidal displacement amplitude, A , in a channel through a fixed matrix. The fluid carries heat or a chemical substance, to which we generically refer as the "tracer." The immobile phase may be sorbed on the channel wall (Fig. 1(a)) or held in the stagnant porosity of the matrix (Fig. 1(b)). The time-average concentration of the tracer increases with distance according to a linear gradient.

[Fig. 1 here]

We define the capacity of the channel, V_c , as the quantity of tracer held in the moving fluid per unit concentration of the moving fluid, per volume of soil. This is simply the porosity occupied by mobile fluid. The capacity of the matrix, V_m , is defined as the quantity of tracer held in the matrix *per unit concentration of the moving fluid*, per volume of soil. For example, if the immobile phase were stagnant fluid, the matrix capacity would be the porosity occupied by that stagnant fluid. If the tracer were linearly sorbed on the matrix, the matrix capacity would be the product of the partition coefficient and the soil density. For a vapor tracer with no sorbed or dissolved phases, V_c and V_m would be the air-filled porosities in the channel and matrix, respectively.

2.2 Concentrations as functions of time

Consider an infinitesimally wide element of fluid in the channel as illustrated in Fig. 1. The sinusoidal displacement of this element of fluid is

$$x = A \sin(\omega t) . \quad (1)$$

At any position, x , we assume that the concentrations of the moving fluid element in the channel and of the immobile adjacent matrix, C_c and C_m , equilibrate according to rate constants τ_c and τ_m . τ_c represents the time in which the concentration in the channel would exponentially approach a constant concentration in an adjacent matrix of infinite capacity; likewise, τ_m represents the time in which the concentration in the matrix would approach the constant concentration in an adjacent channel of infinite capacity. See Appendix A for additional clarification of τ_m and τ_c . The concentrations of the two phases change in time according to:

$$\frac{\partial C_c}{\partial t} = \frac{1}{\tau_c} [C_m(x,t) - C_c(x,t)] , \text{ and} \quad (2a)$$

$$\frac{\partial C_m}{\partial t} = \frac{1}{\tau_m} [C_c(x,t) - C_m(x,t)] . \quad (2b)$$

Eqs.(2a) and (2b) are a form of the rate-limited mass transfer, as presented by Jury and Horton (2004) for a mobile-immobile water model. Tracer gain by the channel must equal loss by the matrix:

$$V_c \frac{\partial C_c}{\partial t} = -V_m \frac{\partial C_m}{\partial t} , \quad (3)$$

which leads to

$$\frac{\tau_m}{\tau_c} = \frac{V_m}{V_c} \quad (4)$$

and

$$\frac{\partial C_c}{\partial t} = -\frac{\tau_m}{\tau_c} \frac{\partial C_m}{\partial t} . \quad (5)$$

We seek steady state solutions of the form:

$$C_c = C_0 + a_c \sin(\omega t + \eta_c) \quad (6a)$$

$$C_m = C_0 + \gamma x + a_m \sin(\omega t + \eta_m) , \quad (6b)$$

in which a_c represents the amplitude of concentration change *in the moving infinitesimal element of fluid*, and a_m represents the amplitude of periodic change of concentration at any immobile location x along the matrix. C_0 represents the equilibrium matrix concentration at the arbitrary location $x = 0$, and γ is the concentration gradient. The phase shifts η_c and η_m describe the concentration changes relative to the phase of the fluid displacement.

Solution of the previous equations leads to:

$$a_c = \frac{\gamma A}{\sqrt{(\omega\tau_c)^2 + (1 + \tau_c/\tau_m)^2}} , \quad (7)$$

$$\eta_c = \text{Tan}^{-1} \left[\frac{-\omega\tau_c}{\left(1 + \tau_c/\tau_m\right)} \right] , \quad (8)$$

$$a_m = a_c \tau_c / \tau_m , \quad (9)$$

$$\eta_m = \eta_c + \pi . \quad (10)$$

Eqs. (9) and (10) show that the concentrations in the matrix and channel vary oppositely in phase, with amplitudes inversely proportional to their relative capacities.

The system is analogous to a resistance-capacitance electrical network, with voltage analogous to chemical concentration. As outlined in Appendix A, when two or more immobile phases exist, their different capacities and equilibration rates combine to act as a single immobile phase, just as parallel linear circuits act as a single equivalent circuit. Therefore, Eqs. (1) through (10) apply equally well to a system with more than one immobile phase--for example, a system with a vapor transported by air, an immobile phase of vapor in stagnant air-filled porosity, and additional immobile phases dissolved in pore water and sorbed on soil.

2.3 Longitudinal flux in the channel

The net longitudinal flux in the channel (quantity per cross-sectional area per time) is the integral of the product of velocity and concentration over one cycle at $x=0$, divided by the period of the cycle:

$$\begin{aligned}
 F &= \frac{1}{T} \int_0^T [a_c \sin(\omega t + \eta_c) - A \gamma \sin(\omega t)] * A \omega \cos(\omega t) dt \quad , \\
 &= \frac{\gamma A^2}{2\tau_c} * \frac{(\omega\tau_c)^2}{(\omega\tau_c)^2 + (1 + \tau_c/\tau_m)^2} \quad .
 \end{aligned} \tag{11}$$

The ratio of channel flux to concentration gradient, F/γ , may be regarded as a diffusivity in the channel, D_e , which we call the "exchange diffusivity" because it depends on the rate of exchange between the channel and matrix:

$$D_e \equiv F/\gamma = \frac{A^2}{2\tau_c} * \frac{(\omega\tau_c)^2}{(\omega\tau_c)^2 + (1 + \tau_c/\tau_m)^2} \quad . \tag{12}$$

We expect the channel capacity will usually be smaller than the matrix capacity, making $\tau_c/\tau_m < 1$. In that case, as the angular frequency becomes large ($\omega\tau_c \gg 1$), the exchange diffusivity approaches $A^2/2\tau_c$, suggesting that a large rate of transport might be achieved by combining a sufficiently large frequency with a small τ_c . Indeed, this has been observed for flow in small pipes (Kurzweg and de Zhao, 1984), but, as a practical consideration for porous media, we caution that the mechanical power to generate a particular displacement amplitude increases with the square root of the frequency (Neeper, 1991). Tortuosity is not explicit in Eq. (12). However, the exchange diffusivity includes the effects of tortuosity because the displacement amplitude represents a straight-line movement of the fluid and transport of tracer, whether or not the flow actually follows a tortuous path.

2.4 Exchange diffusivity applied to gas flow in plane geometry

For ease in comparing equations, equation numbers relating to plane flow will be appended with the letter X, while corresponding equation numbers relating to cylindrical flow will be appended with the letter R.

We consider compressible gas flow in porous media driven by pressure variations that are much smaller than the unchanging average pressure, P_0 . For plane pressure penetration in a semi-infinite medium, as might occur due to barometric pressure cycles at ground surface, the local pressure amplitude P_x and displacement amplitude A_x decrease exponentially with distance X

from the source of oscillatory pressure of amplitude P_s . (see, for example, Neeper, 2002). (Note the distance from the surface of the medium, X , should not be confused with x , the instantaneous displacement of a particular element of gas from its equilibrium position as described in Eq.(1).) Where ϕ_a and ϕ_c are the total gas-filled porosity and gas-filled porosity in the channel, respectively, and other symbols have customary meanings as defined in the notation at the end of this paper, from Darcy's law the penetration of small a sinusoidal pressure is

$$P_x = P_s \exp(-X/\delta) \quad , \quad (13X)$$

in which the exponential penetration depth, δ , is given by

$$\delta = \sqrt{\frac{2kP_0}{\omega\mu\phi_a}} \quad . \quad (14)$$

As explained in Appendix B, for sufficiently small P_x , the plane displacement amplitude in the channel is approximately

$$A_x = \frac{1}{\phi_c} \sqrt{\frac{k\phi_a}{\omega\mu P_0}} P_s \exp(-X/\delta) = \frac{1}{\sqrt{2}} \left(\frac{\phi_a}{\phi_c}\right) \frac{P_x}{P_0} \delta \quad . \quad (15X)$$

The value of δ varies greatly for barometric components penetrating into soils. For example, with P_0 of 1.0e5 Pascals, an air-filled porosity of 0.4, a period of 1 day, and a permeability of 1.0e-12 m², δ would be approximately 19 m. However, if the period were 16 days and the permeability 8.0e-12 m², δ would be approximately 220 m.

From Eqs.(12) and (15X), the exchange diffusivity in the channel at a distance X from the plane pressure source (e.g. below ground surface) is

$$D_{ex} = \left[\frac{1}{2} \frac{\phi_a}{\phi_c^2} \frac{k}{\mu} \frac{P_s^2}{P_0} \exp(-2X/\delta) \right] \left[\frac{\omega\tau_c}{(\omega\tau_c)^2 + (1 + \tau_c/\tau_m)^2} \right] \equiv [F_{HX}][F_E] \quad . \quad (16X)$$

When expressed in terms of the local pressure amplitude P_x at depth X , Eq.(16x) becomes

$$D_{eX} = \left[\frac{1}{2} \frac{\phi_a}{\phi_c^2} \frac{k}{\mu} \frac{P_X^2}{P_0} \right] \left[\frac{\omega \tau_c}{(\omega \tau_c)^2 + (1 + \tau_c / \tau_m)^2} \right] . \quad (17X)$$

The symbolic factors, F_{HX} and F_E of Eq.(16X) represent the exchange diffusivity as a product of a hydraulic term and an equilibration term. Fig. 2 presents the frequency dependence of the equilibration term, F_E . The maximum flux occurs when $\tau_m \gg \tau_c$ and $\omega \tau_c = 1$. In physical terms, the maximum occurs when the matrix has large capacity and the period of motion equals the channel equilibration time multiplied by 2π . The peak value of F_E decreases and shifts toward higher frequencies as the matrix capacity is reduced.

[Fig. 2 here]

2.5 Exchange diffusivity applied to cylindrical gas flow

Cylindrical flow occurs when either extraction or injection wells are operated in a uniform geologic formation. Small amplitude sinusoidal cylindrical gas flow is described by equations analogous to (13X), (15X), (16X), and (17X) (Neeper 2003). The pressure amplitude, P_R , at any particular radius, R , from a borehole of radius R_b , is given by:

$$P_R = P_s \frac{N_0(Z)}{N_0(Z_b)} , \quad (13R)$$

in which N_0 is the magnitude of the modified Bessel function of zero order with argument Z , and

$$Z = \sqrt{2} R / \delta ; \quad Z_b = \sqrt{2} R_b / \delta . \quad (18)$$

(See the table of notation at the end of this paper.) As explained in Appendix B, the radial displacement amplitude is approximately

$$A_R = \frac{1}{\phi_c} \sqrt{\frac{k \phi_a}{\omega \mu P_0}} P_s \frac{N_1(Z)}{N_0(Z_b)} = \frac{1}{\sqrt{2}} \frac{\phi_a}{\phi_c} \frac{P_R}{P_0} \frac{N_1(Z)}{N_0(Z)} \delta , \quad (15R)$$

and the exchange diffusivity in the radial channel is

$$D_{eR} = \left[\frac{1}{2} \frac{\phi_a}{\phi_c^2} \frac{k}{\mu} \frac{P_s^2}{P_0} \frac{N_1^2(Z)}{N_0^2(Z_b)} \right] \left[\frac{\omega \tau_c}{(\omega \tau_c)^2 + (1 + \tau_c / \tau_m)^2} \right] \equiv [F_{HR}][F_E] \quad (16R)$$

When expressed in terms of the local pressure amplitude, P_R , Eq. (16R) becomes

$$D_{eR} = \left[\frac{1}{2} \frac{\phi_a}{\phi_c^2} \frac{k}{\mu} \frac{P_R^2}{P_0} \frac{N_1^2(Z)}{N_0^2(Z)} \right] \left[\frac{\omega \tau_c}{(\omega \tau_c)^2 + (1 + \tau_c / \tau_m)^2} \right] \quad (17R)$$

The equilibration factor F_E is identical in Eqs. (16X) and (16R), but the greater displacement amplitude near a borehole can cause F_{HR} in cylindrical systems to be much larger than the corresponding F_{HX} in plane geometry. Fig. 3 compares the exponential term in F_{HX} with the N_1/N_0 term in F_{HR} , showing that, for distances within $0.1 \cdot \delta$ of the pressure source, *the exchange diffusivity will be much greater in cylindrical flow than in plane flow.*

[Fig. 3 here]

2.6 Comparing exchange diffusivity with mechanical dispersion

Values of the plane hydraulic term, F_{HX} , vary from $9.0e-9$ to $3.0e-3$ m²/s for the following range of soil properties and pressure amplitudes: $0.3 < \phi_a < 0.5$; $0.02 < \phi_c < 0.5$; $1.0e-11 < k < 1.0e-12$ m²; and $100 < P_x < 1000$ Pa. For the more porous soils or larger local pressure amplitudes, F_{HX} is larger than the binary diffusivity of many volatile hydrocarbons in air. Therefore, barometric pumping by the mobile-immobile mechanism may be important, or even dominant, in dispersing subsurface vapors if significant barometric periods are comparable with τ_c .

In practical measurements, the exchange diffusivity and mechanical dispersion are inseparable, as both add to the chemical diffusivity to form a total diffusivity. The value of the exchange diffusivity is given in general by Eq. (12). The mechanical dispersion, equivalent to a diffusivity, is given by

$$D_{mech} = \alpha v, \quad (19)$$

in which v is the fluid velocity in the channel. For a sinusoidal flow, the average magnitude of the velocity is

$$v = \left(\frac{2}{\pi} \right) \omega A \quad (20)$$

In either a plane or cylindrical geometry, the ratio of exchange diffusivity to mechanical dispersion becomes

$$\frac{D_{eX}}{D_{mech}} = \frac{D_{eR}}{D_{mech}} = \frac{\pi A}{4\alpha} F_E \quad . \quad (21)$$

The maximum possible value of F_E is 1/2. Therefore, it is possible that D_{eX} and D_{eR} might be larger than D_{mech} if

$$\frac{A}{\alpha} > \frac{8}{\pi} \quad . \quad (22)$$

This is a necessary, but not sufficient, condition. For example, when $F_E = 1/4$, A/α must be larger than $16/\pi$ if the exchange diffusivity is to exceed mechanical dispersion.

Auer, et al., (1996) predicted significant contributions to vapor plume dispersal by plane barometric pumping from ground surface, assuming values of α of 0.1 or 0.2 m derived from measurements with liquids. However, Mahieu, et al., (2008) recommended values of $\alpha \leq 0.07$ m for gas flows. With $\alpha \leq 0.07$ m, Eq.(21) indicates that the advective exchange diffusivity may exceed the mechanical dispersion in many situations when the period is greater than one day and the permeability is greater than $1.0e-12$ m². This is particularly true when flow occurs in preferential channels, increasing the displacement amplitude as given by Eqs.(15X) and (15R). (See Appendix C regarding possible errors in the Auer paper.)

3. Comparison of analytic theory with numerical simulation

3.1 Soil column in plane geometry, single frequency

We used the FEHM numerical transport code to simulate oscillatory flow and transport as a test of the analytic theory and to explore its implications. The FEHM code allows gas flow, saturated and unsaturated water flow, time-dependent pressure and concentration boundary conditions, and multiple chemical tracers with different sorption characteristics and solubility. Tracers do not affect the gas or water motion. FEHM has been utilized extensively for vadose zone simulations. See, for example, Zyvaloski et al., 1997; Stauffer, et al., 2009; or Chaudhuri, et al., 2009.

Our initial test simulation represented a one-dimensional soil column of one meter length, in which air flow was generated by sinusoidal pressures applied at opposite ends of the column.

The sinusoidal pressure amplitudes and phases were programmed to cause the same flow that would occur in a semi-infinite length of soil with pressure applied at one end. A minor steady pressure gradient was applied to inhibit unidirectional flow (see Appendix B). The permeability was $1.1\text{E-}12\text{m}^2$.

Fig. 4 presents a logical diagram of the computational nodes. For this simulation, the lower row of nodes represents a channel, two rows of nodes represents a soil with total porosity 0.5, air-filled porosity of 0.3, and average saturation 0.4. [Fig. 4 here]

As indicated by Fig. 4, each matrix node was coupled only to its adjacent channel node, with the combination of both nodes representing a single macroscopic volume of soil. The chemical tracer was an idealized soluble vapor that had no influence on gas pressure or gas motion. The capacity of a channel node for the tracer was its pore volume, while the capacity of a matrix node was its air-filled pore volume plus its volume of water divided by a dimensionless Henry's constant. For this soil column simulation, the Henry's constant was 1.0, generating the same capacity in the matrix water as an equal volume of air. The longitudinal chemical diffusivity (along the channel) was $7.0\text{E-}06\text{ m}^2/\text{s}$, allowing chemical diffusion in parallel with the advective transport. For each simulation, the chemical diffusivity between matrix and channel was artificially set to establish a desired value of τ_c , while the τ_m/τ_c ratio remained constant at 4.0, equal to the ratio of matrix capacity to channel capacity. Advection between the channel and matrix carried little tracer in comparison with diffusion, thus causing a negligible reduction of τ_c .

The initial pressure and concentration distributions in the matrix and channel were set to instantaneous values according to the analytic theory, as would occur in steady-state operation with a concentration difference of $1\text{ mole}/\text{m}^3$ across the 1 meter length of column. The amplitude of gas displacement in the channel was approximately 0.25 m, but decreased slightly with distance from the end with the larger pressure amplitude, according to Eq. (15X). Therefore, to maintain a constant average flux of tracer, the initial concentration gradient was set to increase slightly with distance. The magnitudes and phases of tracer concentration at the end boundaries were programmed to vary sinusoidally in time according to the analytic theory, with a one-day period.

Fig. 5 compares the quantity of tracer transported by the soil column during 10 days of operation, as predicted by the FEHM simulation and by the analytic theory. In the numerical simulation, the total transport of tracer is due to a combination of the oscillatory advection, chemical diffusion,

and numerical dispersion. The simulated oscillatory advective transport presented in Fig. 5 is the total production of tracer, minus the presumed chemical diffusion and numerical dispersion, calculated according to the average gradient. As explained in Appendix D, the numerical dispersion was measured as equivalent to a diffusivity of $6.0\text{eE-}08\text{ m}^2/\text{s}$, which is small compared to the binary chemical diffusivity of $7.0\text{e-}06\text{ m}^2/\text{s}$. Fig. 5 shows that the advective production by FEHM was slightly greater than predicted by analytic theory, with the difference being 4% near the peak of the curve. In simulations of the soil column, the advective transport was only 12% of the total production at the peak of the curve, and only 2% of the total at the largest value of $\omega\tau_c$. Thus, it is not surprising to find a small systematic difference between the numerical and analytic values of the oscillatory advective transport. The near-agreement between the numerical results and the analytic theory provides confidence in our subsequent simulations of barometric pumping in cylindrical geometry, where the oscillatory transport can be dominant. [Fig. 5 here]

3.2 Cylindrical flow driven by a barometric spectrum of frequencies

To examine whether the barometric spectrum of pressures would enhance passive extraction at a borehole, we ran a set of simulations in cylindrical geometry, representing soil extending to 100 m radius around a borehole of 0.1 m radius. The initial uniform concentration of the tracer in the pore gas was 1 mole/m³. The applied pressure in the borehole represented an annual atmospheric pressure history at Los Alamos, minus the damped and delayed pressure penetrating vertically from ground surface to a depth of 40 m in a soil with a vertical permeability of $1.0\text{e-}12\text{ m}^2$. The use of such an effective pressure history in the borehole was discussed by Neeper (2003) and Rossabi (2006). The porosities and saturation were as described in Section 3.1, but the capacity ratio τ_m/τ_c was fixed at 6.0 with a Henry's constant of 0.5. The chemical diffusivity for longitudinal transport in the channel was $4.0\text{eE-}6\text{ m}^2/\text{s}$, and the radial permeability was $1.6\text{e-}12\text{ m}^2$. This value of permeability was chosen to represent a situation that would be marginally acceptable for PSVE. Soils with permeability smaller than $1.0\text{e-}12\text{ m}^2$ are sometimes unsuitable for vapor extraction (Burke, et al., 2000). Thus, these simulations explore barometric pumping with permeability near the lower limit for which passive vapor extraction might be considered practical.

Multiple tracers, each with a different τ_c value imposed by an artificial value of diffusivity between the matrix and

channel, were simulated with repeating one-year cycles of the same pressure history. The variation of τ_c was a means for testing the range of equilibration times for which barometric spectrum might be beneficial.

Fig. 6 shows the moles of tracer produced per length of borehole as a function of $2\pi\tau_c$, a convenient unit of equilibration time equal to the oscillatory period at which $\omega\tau_c$ equals 1. The lower two curves of Fig. 6 display production with no flow, when transport is due only to retarded diffusion in the channel. Without flow, the production by chemical diffusion would be approximately three times larger if the soil had single porosity, thereby allowing radial transport by diffusion in all of the air-filled porosity.

[Fig. 6 here]

The upper two curves of Fig. 6 show production with barometric flow, with and without mechanical dispersion. A mechanical dispersivity of 0.07 m increased the production by at most 1%, confirming that the peak of production is due to the exchange mechanism. Production peaks when $2\pi\tau_c$ is approximately 17 days, or τ_c is approximately 2.7 days; however, the exchange mechanism appreciably increases the production for values of $2\pi\tau_c$ between 1 and 1,000 days. This numerical example demonstrates that cylindrical barometric pumping can be important if τ_c is between 0.16 and 160 days. Such equilibration times occur in actual soils. For example, Nadim, et al. (1997) measured equilibration times between two and ten days for trichloroethylene in soil columns. Thus, the effective barometric spectrum may be quite suitable for PSVE in many soils. The F_{HX} and F_{HR} terms in Eqs. (16X) and (16R) increase nonlinearly with radial permeability and inversely with the square of the channel porosity, suggesting that the oscillatory advective transport would be even more pronounced in a more permeable soil, or in a soil with a smaller channel porosity.

3.3 *The exchange diffusivity as a computational device*

Applying the multiple frequency components of the barometric spectrum to Eq. (16R) will generate multiple terms of exchange diffusivity at any specific distance from a borehole. As discussed in Neeper (2001) and in Appendix E, these multiple terms can be added linearly to form a single effective value of the exchange diffusivity at any radius. It should therefore be possible to estimate the transport of a tracer using a diffusion calculation, eliminating the need to simulate the fluid flow at every instant throughout the months or years of interest. The exchange diffusivity does not provide an estimate of the

instantaneous flux. Instead, it relates to the average value of the flux throughout the longest cycle of fluid motion. Barometric flows include cycles longer than 7 days. Therefore, we expect that transport predicted by the exchange diffusivity over an interval of months will be approximately equal to the more exact value predicted by a complete simulation including fluid flow.

3.3.1 Comparison of exchange diffusivity with simulation

Figure 7 shows the exchange diffusivity as a function of radius for the barometric spectrum and soil properties of the simulation described in Section 3.2. Fig. 7 also shows the total diffusivity, which is the sum of the exchange diffusivity and the chemical diffusivity of $4.0\text{E-}6 \text{ m}^2/\text{s}$.

[Fig. 7 here]

To compare an estimate using exchange diffusivity with simulation, we ran a calculation identical to that of Section 3.2 for $2\pi\tau_c = 16.791$ days, but with the total diffusivity (exchange plus chemical) applied to the channel while the gas was held immobile. Fig. 8(a) compares contours of concentration in the matrix after 1 and 10 years, as calculated by the complete simulation and by the total diffusivity without flow. Fig. 8(b) compares the tracer produced at the borehole as a function of time. The exchange diffusivity closely replicates the transport of tracer, underestimating the production at ten years by 2.8%.

[Fig. 8 here]

3.3.2 Application of the exchange diffusivity as a design tool

In Fig. 7, it is apparent that, for the pressure spectrum and soil of this problem, the exchange diffusivity is insignificant at any radius larger than 10 m. This does not imply that the so-called radius of influence of the passive borehole is 10 m. In fact, most of the tracer removed during ten years originated at a radius larger than 10 m. The chemical diffusivity, combined with the large circumferential area at a radius greater than 10 m is adequate to maintain the flux carried by the exchange diffusivity at a smaller radius.

Manipulation of terms in Eq. (16R) will show that the radial exchange diffusivity is approximately proportional to the square of the permeability. Thus, increasing the permeability from 1.6 to 16 Darcies would increase the exchange diffusivity in Fig. 7 by two orders of magnitude.

For this example, we calculated the value of the exchange diffusivity sum over frequency components at each radial node of

the corresponding simulation. The Bessel functions in F_{HR} of Eq. (16R) might make such a calculation onerous for practical applications. As shown in Fig. 7, the exchange diffusivity varies approximately with the inverse of the square of the radius. This is because, for significant frequency components of the barometric spectrum, almost the same volume flow of air occurs at any radius less than 10 m. For a design tool, it would usually be adequate to calculate the sum of exchange diffusivity frequency components at only one value of radius, and then apply a $1/R^2$ dependence to obtain values elsewhere.

4. Is the exchange diffusivity a practical concept?

Values of the soil properties ϕ_c , τ_c , and τ_m are not usually known. Therefore, it is reasonable to ask whether the theory can be applied to practical situations. Although dual porosity increases the exchange diffusivity, we emphasize that the theory does not require a dual porosity. In an ideal soil with uniform flow in all porosity, ϕ_c would simply be equal to ϕ_a . However, situations represented by dual porosity occur frequently in the literature. For example, Selker, et al. (1999) review preferential flow, and Brusseau (1994) extensively reviews the dual porosity model. The channel porosity, ϕ_c , might be estimated in the field by tests with inert tracer gas (Marley, et al. 1992; Barna, 1995), by curve-fitting of a few weeks of PSVE test data (Neeper and Stauffer, this issue), or, for saturated systems, by leaching tests (Kamra, et al. (2001)).

Estimates of τ_c and τ_m can be derived if the capacities and rate constants are known, but one must be aware that sorbed capacity may depend on competing contaminants and moisture content (Poulsen, et al., 1998). Although the immobile (matrix) capacity may be quantitatively uncertain, it is usually much larger than the mobile (channel) capacity, in which case τ_c/τ_m would be small. τ_c might then control the rebound of concentration after a temporary active extraction (Switzer and Kosson, 2007). Soil properties can also be discerned from laboratory breakthrough curves (Brusseau, 1994; Brusseau et al., 2010).

The permeability and air-filled porosity should be known before any SVE system is designed. The parameters ϕ_c , τ_c , and τ_m do not imply that the theory applies only to soil with a dual porosity. If values of τ_c and ϕ_c can be estimated by the means suggested above or other methods, then the theory would be practical for guiding the design and predicting the performance of a PSVE system. When the concept of the exchange diffusivity is applied to a set of barometric pressure amplitudes using

Eqs. (16X) and (16R), the investigator must remember that a diffusion calculation predicts only the average transport throughout a time interval long enough to contain all significant frequency components of the effective barometric spectrum at the subsurface depth of interest.

5. Review and conclusions

This paper presented an analysis of the unidirectional transport of chemicals or heat by oscillatory flow of a fluid in a porous medium. The transport mechanism occurs when the heat or chemical equilibrates with an immobile phase via any rate-limited process. The transport is independent of the exact nature of exchange, but maximum transport occurs when the period of fluid motion is close to the equilibration time of the moving fluid multiplied by 2π . Transport by this mechanism can exceed the transport by chemical diffusion or by mechanical dispersion. It was shown that the transport can be expressed in terms of an exchange diffusivity, which predicts approximately the same average transport rate as a detailed simulation of fluid motion with kinetic mass transfer. When the flow is driven by multiple frequencies, the individual frequency components of exchange diffusivity add linearly to form a single, larger value of exchange diffusivity.

All examples presented here featured chemical transport by air as the moving fluid, with the immobile phase provided by vapor in stagnant air-filled porosity combined with dissolution in stagnant pore water. These examples were chosen to illustrate application of the transport mechanism for passive soil vapor extraction. However, similar examples could be made using periodic flow of water with an immobile phase of solute provided by stagnant porosity or by rate-limited sorption.

Oscillatory transport was evaluated for barometric pressure cycles. Finite element simulation of plane flow in a soil column produced transport in agreement with the analytic theory. Simulation of cylindrical flow showed that a barometric pressure spectrum is appropriate for passive extraction in soils with equilibration times in the range of 0.16 to 160 or more days. Other configurations with single porosity were not evaluated.

The rate of transport induced by the oscillatory mechanism is proportional to the square of the displacement amplitude of the fluid. The dual porosity presumed in the examples causes a larger displacement amplitude than would occur with uniform flow in all porosity, thereby increasing the transport. The dual porosity is a simplified representation of various flows in multiple channels. However, it is not an artifice, as flow in preferential channels may be the rule more than the exception in

heterogeneous soils or fractured media. See, for example, Selker, et al., 1999; and Kamra, et al., 2001.

Notation

Units are examples appropriate for chemical transport.

A	Displacement amplitude of periodic fluid motion (m).
C	Concentration (moles/m ³)
D	Diffusivity (m ² /s)
F	Flux (moles/m ² s)
F_{HX} F_{HR}	Hydraulic terms in expressions for exchange diffusivity.
F_E	Equilibration term in the exchange diffusivity.
N_0	Magnitude of modified Bessel function, zero order.
N_1	Magnitude of modified Bessel function, first order.
P	Pressure (Pa).
R	Radius (m).
T	Period of oscillation (s).
V	Capacity, expressed as an equivalent volume.
X	Distance from source of pressure in plane flow (m).
Y	Peak concentration (moles/m ³).
W	Peak width (m).
Z	$\sqrt{2} \cdot (R/\delta)$.
a	Amplitude of periodic variation of concentration.
k	Permeability (m ²)
t	Time (s).
v	Fluid velocity (m/s).
x	Displacement of fluid from average position (m).
α	Mechanical dispersivity (m).
γ	Gradient of concentration (moles/m ⁴).
Δ	Half-width of a Gaussian curve at 1/e of peak height (m).
δ	Exponential penetration depth of a periodic pressure (m).
η	Phase angle (radians).
μ	Viscosity (Pa s).
τ	Exponential equilibration time (s).
ϕ	Porosity.
ω	Angular frequency (radians/s).

Subscripts

a	Air, related to air-filled porosity.
b	Borehole.
c	Channel.
e	Relating to exchange diffusivity.
i	Indicating value at time zero or initial location.
m	Matrix.
o	Time-average value.
p	Peak value, maximum value.
R	Relating to cylindrical coordinates.

s Value at source location of a sinusoidal variable.
 w Relating to width.
 X Relating to plane, Cartesian coordinates.

Acknowledgements

Office space and facilities were graciously provided to the first author by the Los Alamos National Laboratory. The second author appreciates support by the U.S. Department of Energy.

Appendix A. Multiple immobile phases

The transport system with oscillating fluid and one or more immobile phases is analogous to an electrical circuit driven by oscillating voltage, as shown in Fig. A1. Electric capacitance is analogous to volume (or equivalent capacity) of the moving and immobile phases. The resistance-capacitance product is analogous to an equilibration time. For example, for a single immobile phase represented by resistance r_1 and matrix capacity V_1 , the channel equilibration time τ_c would be $r_1 * V_c$. Some readers may find it easier to derive the results expressed in Eqs. (7)-(10) by application of circuit theory than by the Eqs. (1)-(6b). Multiple immobile phases act in parallel, as indicated by Fig A1, and can be reduced to a single equivalent resistance and capacitance. Therefore, the theory for a single immobile phase applies to multiple immobile phases.

[Fig. A1 here]

Appendix B. The significance of small amplitude displacement.

Eqs. (15X) through (17R) presume that the spatial displacement of the air is equal to the integral of the velocity at a fixed location and is therefore sinusoidal. However, if the displacement amplitude is significant compared to δ , then the displaced element of air experiences a pressure gradient that varies with position during the cycle and the displacement is not exactly sinusoidal. The pressure gradient is larger as the air moves toward the source of oscillating pressure, leading to a gradual drift away from the source of pressure. This can cause difficulties during numerical modeling (Neeper and Stauffer, 2005). For one-dimensional vertical propagation of barometric pressures from ground surface, a small, steady reversed gradient would eliminate the accumulation of one-way displacement. However, there is no apparent reason why a slow radial movement of air might not progress outward from an open vertical borehole. When the channel porosity is much smaller than the total porosity, the nonlinear movement would have actual displacement amplitudes smaller than predicted by Eqs. (15X) and (15R), leading to predicted values of equilibration diffusivity that are too large.

Appendix C. Possible errors in the paper by Auer, et al. (1996).

Haagenstad (2009) reported that Fig. 3 of the Auer paper may present pore velocity rather than Darcy velocity as labeled.

Also, it appears that the peak absolute value of the velocity, rather than an average absolute value, was used in calculating the mechanical dispersion. These errors do not alter the broad conclusions of the Auer paper.

Appendix D. Measuring numerical dispersion in simulations.

In one-dimensional diffusion, an initial point-like (delta function) distribution of tracer will expand in time, with the concentration becoming a Gaussian distribution in space. In both plane and cylindrical simulations, we utilized a test tracer located initially in only one channel node. Transport of this special tracer into the matrix nodes was prohibited, else spread of the tracer would occur due to oscillatory transport. The tracer had negligible chemical diffusivity; therefore, its spread was solely due to numerical dispersion of the irregular barometric flow.

In plane geometry, an initial narrow spike of concentration C_i of width W_i will diffuse to a profile given by

$$C(X,t) = \frac{C_i(X_i,t) W_i}{2\sqrt{\pi D t}} \exp\left\{-\left[\frac{(X - X_p)^2}{4 D t}\right]\right\} , \quad (D1)$$

in which D is the diffusivity and X_p is the location of the concentration peak at time t . The diffusivity can be deduced from the peak of the distribution according to

$$D_p = \frac{1}{4\pi t} \left(\frac{C_i W_i}{Y}\right)^2 , \quad (D2)$$

in which Y is the height of the peak. Likewise, the diffusivity can be deduced from the half-width at $1/e$ of the peak value of the Gaussian distribution, Δ :

$$D_w = \frac{\Delta^2}{4t} . \quad (D3)$$

In the simulation of the soil column reported in Section 3.1, a spike of tracer was initially located at $X=0.32$ m. Fig. D1 shows the profile of the spike at 1 and 10 days. From the curve at 1 day, the diffusivity values due to numerical dispersion are $D_p = 6.09E-8$ m²/s, and $D_w = 6.00E-8$ m²/s. These values are two orders of magnitude smaller than the chemical diffusivity in the channel ($7.0E-6$ m²/s) during the simulations leading to Fig. 5.

Therefore, we conclude that the results were not seriously affected by numerical dispersion.

[Fig. D1 here]

Fig. D2 displays concentration profiles for tracer spikes initially at radii of 2.50, 4.99, and 7.51 meters in the cylindrical simulations of Section 3.2 and Fig. 6. Even if a spike had no dispersion, its width would expand as it moved to a smaller radius and contract as it moved to a larger radius, because air volume is conserved. Consequently, for cylindrical systems,

$$D_w = \frac{\Delta^2 \left(\frac{R_p}{R_i} \right)^2}{4t} \quad . \quad (D4)$$

Tracer is removed when part of a profile is exhaled from the simulated borehole, as indicated by the distorted curve in Fig. D2 for the tracer initially at 2.50 m radius. The numerical dispersion cannot be estimated accurately from such distorted distributions, limiting the time interval over which this technique is valid. At 70 days, D_p values calculated by Eq. (D2) are 1.1E-7, and 0.8E-7 m²/s, respectively, for the tracers initially located at 4.99 and 7.51 m radius. Eq. (D4) predicts D_w values of 1.1E-7, and 0.9E-7 m²/s, respectively. These values indicate that numerical dispersion did not significantly affect the cylindrical simulations of Section 3.2. Furthermore, in a simulation as long as one year, tracer in the channel at a radius less than 5 m is eventually expelled into the borehole by advection; therefore, numerical dispersion near the borehole does not significantly alter the long term production of tracer. [Fig. D2 here]

Appendix E. Addition of frequency terms in an exchange diffusivity.

According to Eq. (12), the exchange diffusivity depends on the square of the displacement amplitude of the fluid. It might therefore seem that a total diffusivity could not be formed by a linear sum. Furthermore, displacements of various frequency components do not add linearly to form a total displacement, because any displacement will bring a fluid element to a new position, where the phases of the pressure components are different. However, the transport of tracer at a given location depends on the time integral of velocity at that fixed location, as expressed in the integral of Eq. (11). In Eq. (11), a sum of Fourier components of concentration and local displacement will

be orthogonal to all but the corresponding components of velocity, with the result that the flux is a sum of Fourier terms, each with its own local displacement amplitude. See Neeper (2001). In general, an element of fluid will drift away from its initial location, but the exchange diffusivity at a particular location will remain unchanged when averaged over times longer than the window of Fourier components.

Fig. E1 presents a logical flow diagram for calculating the exchange diffusivity and the total diffusivity as a function of radius, as was illustrated in Fig. 7. In Fig E1, calculations are indicated by ellipses, while data or results are indicated by rectangles. FFT indicates a fast Fourier transform. No inverse transform is needed unless the investigator wishes to see the effective pressure history as illustrated in the companion paper (Neeper and Stauffer, this issue). It is not necessary that the original atmospheric pressure data appear in the form of 2^m points per day for 2^n days (n, m are integers). However, this form will preserve the unique components of the atmospheric solar tides, which are harmonics of 1 day.
[Fig. E1 here]

References

- Armstrong, J. E., Frind, E. O., McClellan, R. D., 1994. Nonequilibrium mass transfer between the vapor, aqueous, and solid phases in unsaturated soils during vapor extraction. *Water Resour. Res.* 30, 355-368.
- Auer, L. H., Rosenberg, N. D., Birdsell, K. H., and E. M. Whitney, 1996. The effects of barometric pumping on contaminant transport. *J. Contam. Hydrol.* 24, 145-166.
- Barna, M. G., 1995. The use of sulfur hexafluoride as a vadose zone tracer to investigate active and passive soil vapor extraction. M.S. thesis, Washington State University, Pullman, WA, USA.
- Brusseu, M. L., 1991. Transport of organic chemicals by gas advection in structured or heterogeneous porous media: Development of a model and application to column experiments. *Water Resour. Res.*, 27, 3189-3199.
- Brusseu, M. L. 1994. Transport of reactive contaminants in heterogeneous porous media. *Rev. Geophys.*, 32, 285-313.
- Brusseu, M. L., Rohay, V., and Truex, M. J., 2010. Analysis of soil vapor extraction data to evaluate mass-transfer constraints and estimate source-zone mass flux. *Ground Water Monit. Rem.*, accepted for publication. doi: 10.1111/j1745-6592.2010.001286.x
- Burke, G., Singh, B. R., and Theodore, L., 2000. *Handbook of Environmental Management and Technology*. second edition, Wiley-Interscience, New York.
- Chaudhuri, A., H. Rajaram, H.S Viswanathan , G.A. Zyvoloski, and Stauffer, P.H., 2009. Buoyant convection resulting from dissolution and permeability growth in vertical limestone fractures. *Geophys. Res. Lett.* 36, L03401, doi:10.1029/2008GL036533.
- Choi, J. and Smith, J. A., 2005. Geoenvironmental factors affecting organic vapor advection and diffusion fluxes from the unsaturated zone to the atmosphere under natural conditions. *Environ. Eng. Sci.* 22, 95-107.
- Cirpka, O. A., 2005. Effects of sorption on transverse mixing in transient flows. *J. Contam. Hydrol.* 78, 207-229. doi:10.1016/j.conhyd.2005.05.008.

Ellerd, M. G., Massmann, J. W., Schwaegler, D. P., and Rohay, V. J., 1999. Enhancements for passive vapor extraction: The Hanford study. *Ground water* 37, 427-437.

Haagenstad, M. P., 2009. Private communication.

Jaeger, M. J., and Kurzweg, U. H., 2003. Ventilation of enclosed porous media by the application of periodic pressure variations. *Int. J. Eng. Sci.* 41, 2299-2304.

Jennings, A. A. and Patil, P. 2002. Feasibility modeling of passive soil vapor extraction. *J. Env. Eng. Sci.* 1, 157-172.

Jury, W., and Horton, R., 2004. *Soil Physics*, sixth edition. John Wiley and Sons, Inc. Hoboken, New Jersey USA.

Kamra, S. K., Lennartz, B., Van Genuchten, M. Th., and Widmoser, P., 2001. Evaluating non-equilibrium solute transport in small soil columns. *J. Contam. Hydrol.* 48, 189-212.

Kay, A., 1997. Advection-diffusion in reversing and oscillating flows: 2. Flows with multiple reversals. *IMA J. Appl. Math.* 58, 185-210.

Kurzweg, U. H., Howell, G., and Jaeger, M. J. 1984. Enhanced dispersion in oscillatory flows. *Phys. Fluids* 27, 1046-1048.

Kurzweg, U. H. and de Zhao, L., 1984. Heat transfer by high-frequency oscillations: A new hydrodynamic technique for achieving large effective thermal conductivities. *Phys. Fluids* 27, 2624-2627.

Lal, R. and Shukla, M. K., 2004. *Principles of Soil Physics*. Marcel Dekker, Inc. New York, Basel.

Ma, L., Selim, H. M., 1998. *Physical Nonequilibrium in Soils: Modeling and Application*. Ann Arbor Press, Chelsea, Michigan USA.

Mahieu, K., De Visscher, A., Vanrolleghem, P., and Van Cleemput, O., 2008. Modelling of stable isotope fractionation by methane oxidation and diffusion in landfill cover soils. *Waste Management* 28, 1535-1542.

Marley, M. C., Cody, R. J., Polonsky, J. D., Woodward, D. D., Buterbaugh, G. J., 1992. Application of tracer gas studies in

the optimal design of soil vapor extraction systems. Proc. Sixth National Outdoor Action Conference, Las Vegas, NV, May 11-13, pp543-557.

Nadim, F., Nadim, A., Hoag, G. E., and Dahmani, A. M., 1997. Desorption rate limitation in the extraction of organic molecules from unsaturated soils during soil venting operations. J. Contam. Hydrol. 25, 21-37.

Nilson, R. H., Peterson, E. W., Lie, K. H., Burkhard, N. R., Hearst, J. R., 1991. Atmospheric pumping: A mechanism causing vertical transport of contaminated gases through fractured permeable media. J. Geophys. Res. 96, 21933-21948.

Neeper, D. A., 1991. Soil vapor extraction enhanced by oscillatory flow. Proc. Fifth National Outdoor Action Conf. Las Vegas, NV. pp. 75-88.

Neeper, D. A. 2001. A model of oscillatory transport in granular soils, with application to barometric pumping and earth tides. J. Contam. Hydrol. 48, 237-252.

Neeper, D. A., 2002. Investigation of the vadose zone using barometric pressure cycles. J. Contam. Hydrol. 54, 59-80.

Neeper, D. A., 2003. Harmonic analysis of flow in open boreholes due to barometric pressure cycles. J. Contam. Hydrol. 60, 135-162.

Neeper, D. A. and Stauffer, P., 2005. Unidirectional gas flow in soil porosity resulting from barometric pressure cycles. J. Contam. Hydrol 78, 281-289.

Neeper, D. A. and Stauffer, P. H. (this issue) Transport by oscillatory flow in soils with kinetic mass transfer. II. Field experiment.

Poulsen, T. G., Moldrup, P., Yamaguchi, T., Massmann, J. W., Hansen, J. A., 1998. VOC vapor sorption in soil: Soil type dependent model and implications for vapor extraction. J. Envir. Engrg. 124, 146-156.

Rossabi, J., 2006. Analyzing barometric pumping to characterize subsurface permeability. Gas Transport in Porous Media 20, 279-290. Ho, C., Webb, S., eds. Springer, New York, USA.

Schonewill, P. P., 2008. Oscillatory Flow: Effect on Transverse

Diffusivity and internal migration of particles and bubbles. Ph.D. thesis, Chemical and Biochemical Engineering Department, Notre Dame University, Indiana USA. <http://etd.nd.edu/ETD-db/theses/available/etd-08272008-102042/unrestricted/SchonewillP082008.pdf>

Selker, J. S., Keller, C. K., and McCord, J. T., 1999. Vadose Zone Processes. Lewis Publishers, New York, USA.

Stauffer, P.H., Vrugt, J. A., Turin, H. J., Gable, C.W. and Soll, W. E., 2009. Untangling diffusion from advection in unsaturated porous media: Experimental data, modeling, and parameter uncertainty assessment. Vadose Zone J. 8, 510-522. doi:10.2136/vzj2008.0055.

Switzer, C., Kosson, D., 2007. Soil vapor extraction performance in layered vadose zone materials. Vadose Zone J. 6, 397-405. doi:10.2136/vzj2005.0131.

Wilson, D. J., Rodriguez-Maroto, J. M., Gomez-Lahoz, C., 1995. Soil Cleanup by in-situ aeration 23. Effect of air channeling. Sep. Sci. Technol. 30, 2491-2508.

Zyvaloski, G. A., Robinson, B. A., Dash, Z. V., Trease, L. L., 1997. Summary of the models and methods for the FEHM application: A finite-element heat- and mass-transfer code. Los Alamos National Laboratory report LA-13307-MS, available from the National Technical Information Service, U.S. Department of Commerce, 5285 Port Royal Rd., Springfield, VA 22161, USA. <http://library.lanl.gov/cgi-bin/getfile?00412556.pdf>.

FIGURE CAPTIONS

Fig. 1. (a) Schematic diagram, indicating the small fluid element of Eq. (1), with oscillatory flow in a channel and adsorbed solute on the channel wall. (b) Schematic diagram indicating liquid or gas in stagnant porosity. Concentration increases to the right in both diagrams.

Fig. 2. Plot of FE versus $\omega\tau_c$ for selected values of τ_m/τ_c .

Fig. 3. Variation of the hydraulic terms with distance in cylindrical geometry for two values of R_b/δ , and in plane geometry. F_R varies as the ratio of the $[N_1(R)/N_0(R_b)]^2$, whereas F_x decreases exponentially.

Fig. 4. Logical diagram of the connections between nodes of the finite element simulations.

Fig. 5. Quantity of tracer transported as a function of $\omega\tau_c$, comparing analytic theory with finite element simulation.

Fig. 6. Tracer produced per meter length of borehole in cylindrical geometry as a function of channel equilibration time with and without dispersivity of 0.07 m.

Fig. 7. Barometric exchange diffusivity and total diffusivity versus radius for the conditions of Section 3.2. The exchange diffusivity varies approximately as $1/R^2$.

Fig 8. (a) Air concentration of tracer versus radius at 1 and 10 years after initiation of extraction, as calculated according to the exchange diffusivity with no gas motion, and as calculated by a simulation with flow. (b) Tracer produced per meter of borehole length as a function of time.

Fig. A1. Diagram of analogous electrical circuit with two immobile phases indicated by V_1, r_1 and V_2, r_2 . V_c represents the channel capacity.

Fig. D1. Concentration of spiked tracer versus position along soil column at 1 day and 10 days in the simulation of Section 3.1. The peak height Y and half-width Δ yield estimates of numerical diffusivity.

Fig. D2. Concentration versus radius of three spikes initially at radii of 2.50 m, 4.99 m, and 7.51 m in the simulation of

Section 3.2. Gaussian fits provide estimates of numerical diffusivity.

Fig. E1. Flow chart for calculation of total diffusivity, starting with atmospheric pressure data.

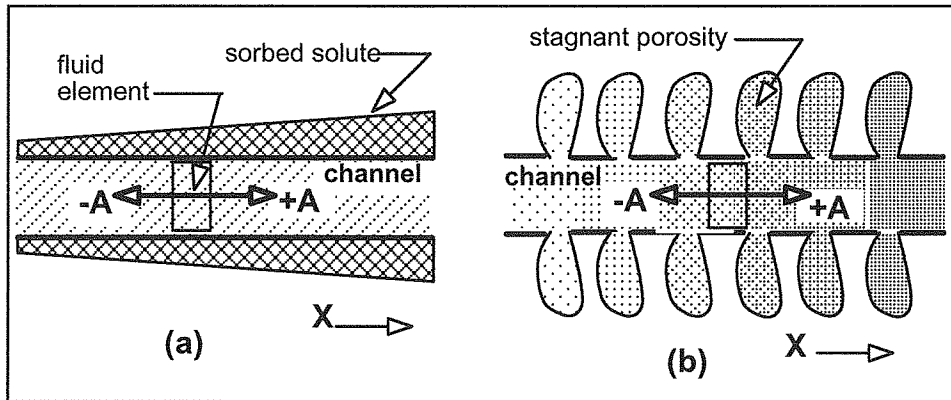


Fig. 1. (a) Schematic diagram indicating the small fluid element of Eq. (1), with oscillatory flow and adsorbed solute on the channel wall. (b) Schematic diagram indicating liquid or gas in stagnant porosity. Concentration increases to the right in both diagrams

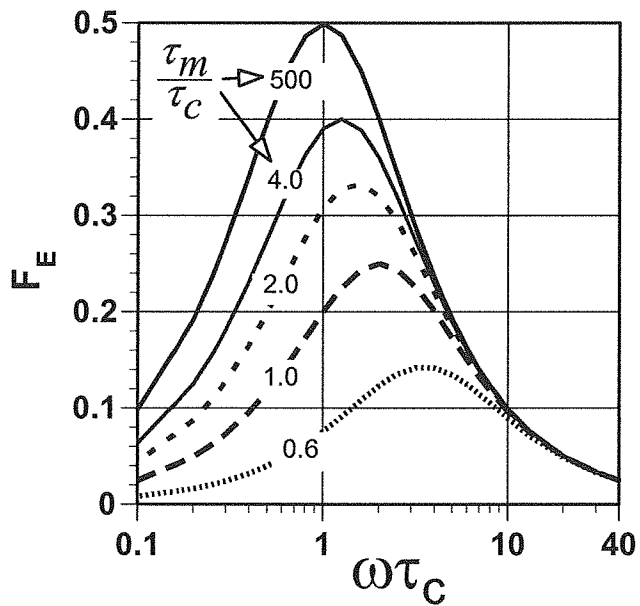


Fig. 2. Plot of FE versus $\omega\tau_c$ for selected values of τ_m/τ_c .

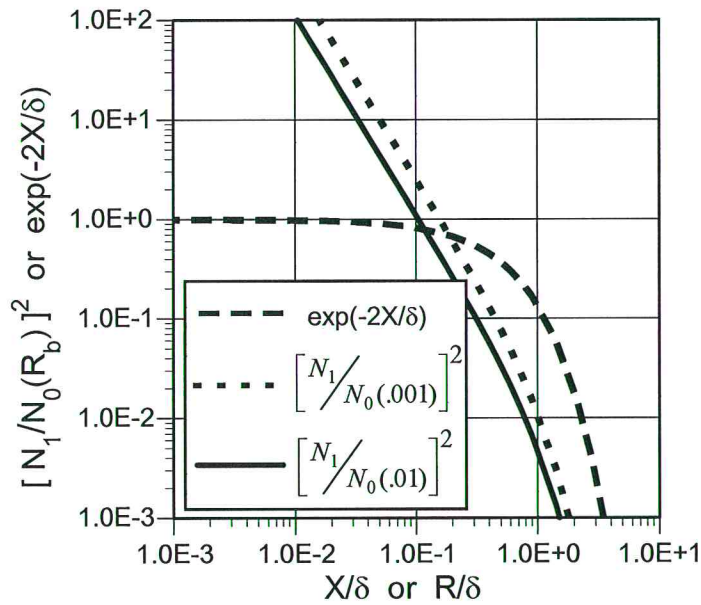


Fig. 3. Variation of the hydraulic terms with distance in cylindrical geometry for two values of R_b/δ , and in plane geometry. F_R varies as the ratio of the $[N_1(R)/N_0(R_b)]^2$, whereas F_X decreases exponentially.

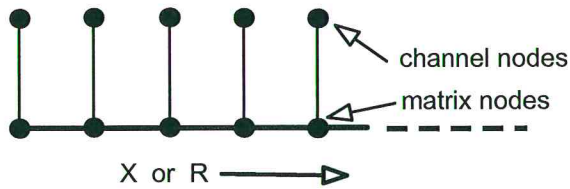


Fig. 4. Logical diagram of the connections between nodes of the finite element simulations.

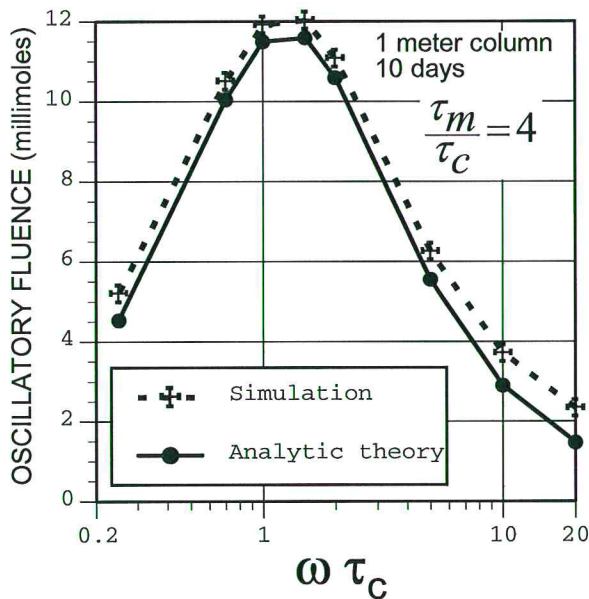


Fig. 5. Quantity of tracer transported as a function of $\omega\tau_c$, comparing analytic theory with finite element simulation.

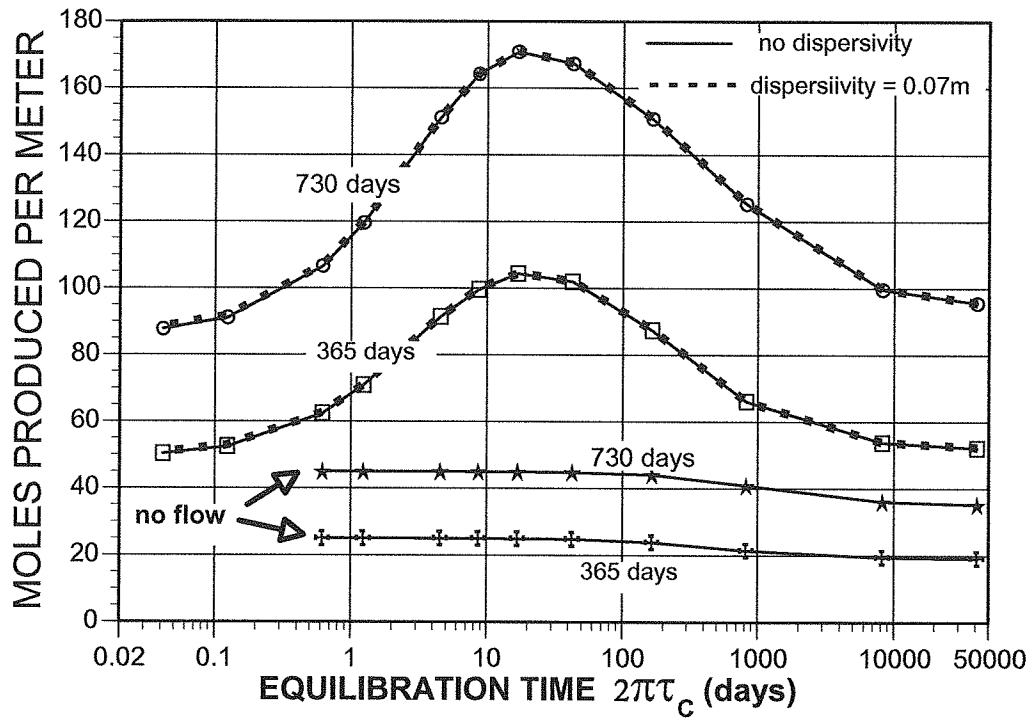


Fig. 6. Tracer produced per meter length of borehole in cylindrical geometry as a function of channel equilibration time with and without dispersivity of 0.07 m.

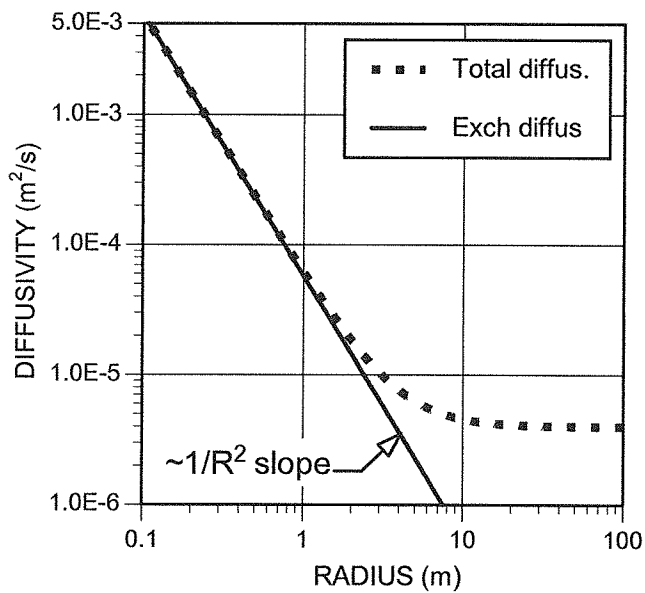


Fig. 7. Barometric exchange diffusivity and total diffusivity versus radius for the conditions of Section 3.2. The exchange diffusivity varies approximately as $1/R^2$.

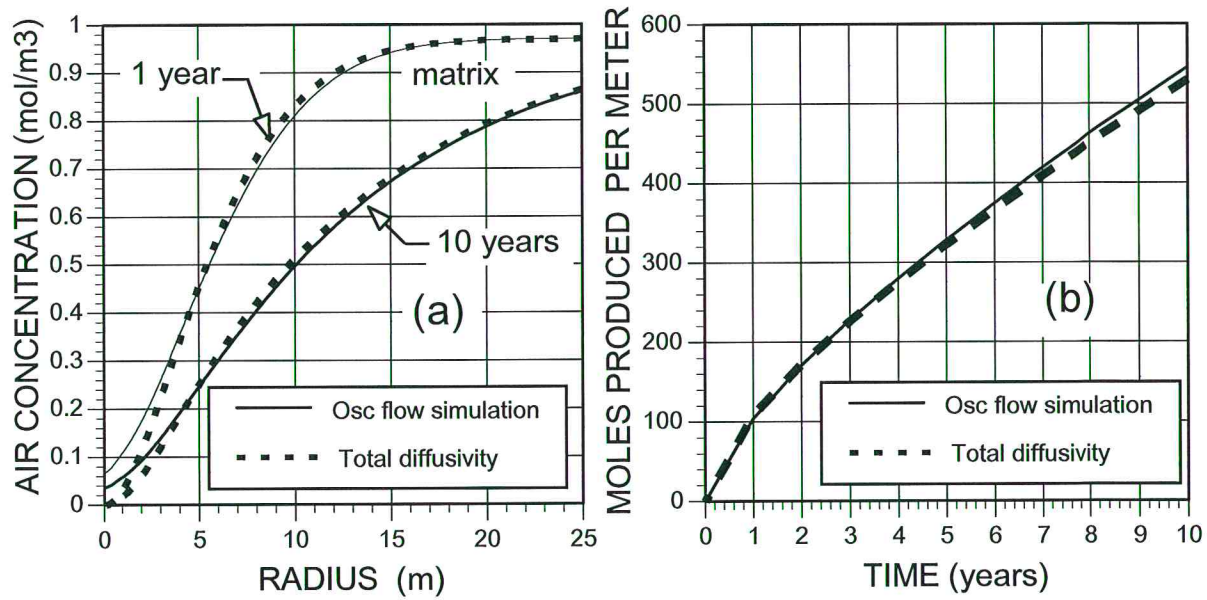


Fig 8. (a) Air concentration of tracer versus radius at 1 and 10 years after initiation of extraction, as calculated according to the total diffusivity with no gas motion, and as calculated by a simulation with flow. (b) Tracer produced per meter of borehole length as a function of time.

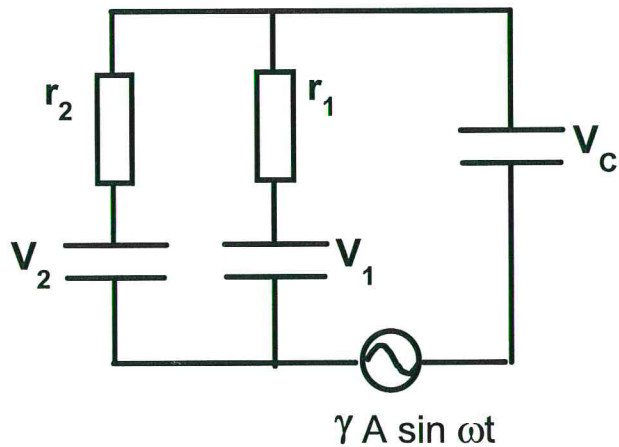


Fig. A1. Diagram of analogous electrical circuit with two immobile phases indicated by V_1 , r_1 and V_2 , r_2 . V_c represents the channel capacity.

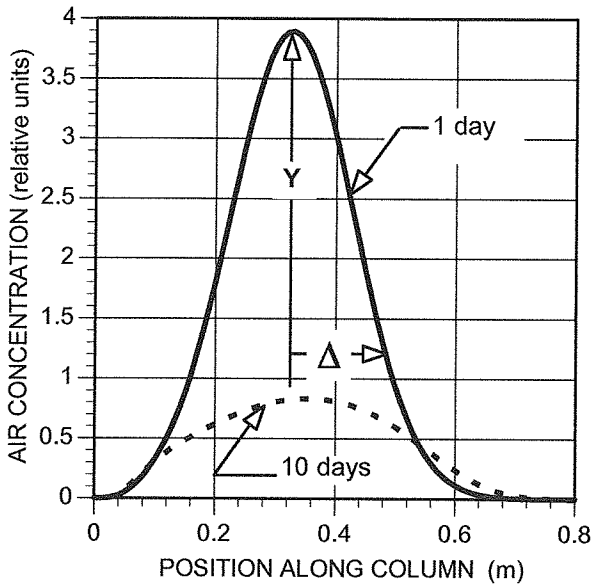


Fig. D1. Concentration of spiked tracer versus position along soil column at 1 day and 10 days in the simulation of Section 3.1. The peak height Y and half-width Δ yield estimates of numerical diffusivity.

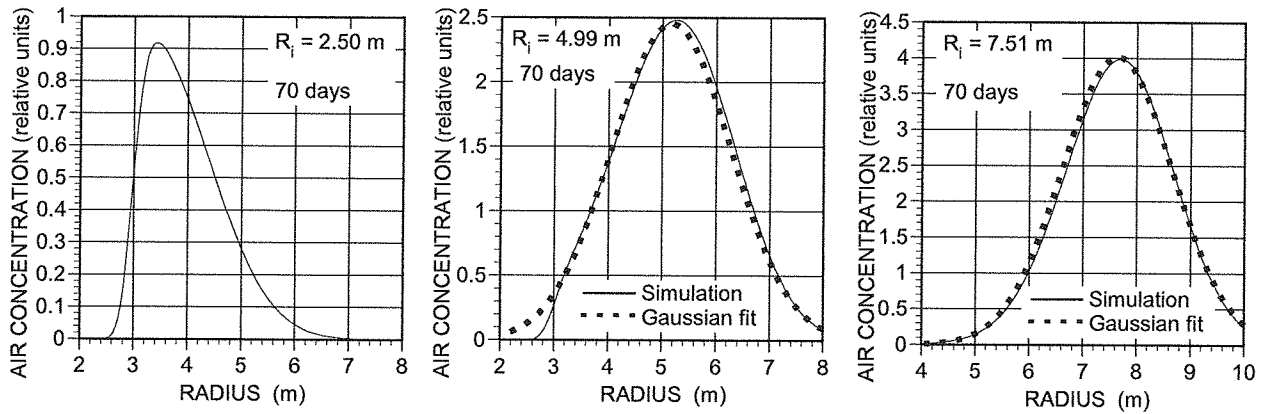


Fig D2. Concentration versus radius of three spikes initially at radii of 2.50 m, 4.99 m, and 7.51 m in the simulation of Section 3.2. Gaussian fits provide estimates of numerical diffusivity.

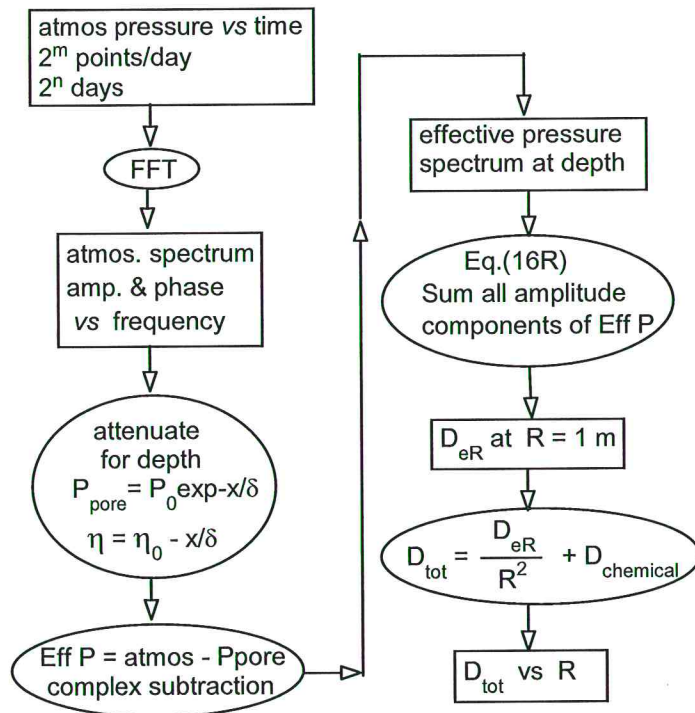


Fig. E1. Flow chart for calculation of total diffusivity, starting with atmospheric pressure data.